Chinese Journal of Aeronautics, (2023), 36(4): 120–133

Chinese Society of Aeronautics and Astronautics
& Beihang University

Chinese Journal of Aeronautics

cja@buaa.edu.cn
www.sciencedirect.com

Direct thrust test and asymmetric performance of porous ionic liquid electrospray thruster

Yuntao GUO [a], Wei SUN [a], Zhenning SUN [b], Zhiwen WU [a,*], Jianwu HE [c,d], Chao YANG [c,d], Ningfei WANG [a]

[a] School of Aerospace Engineering, Beijing Institute of Technology, Beijing 100081, China
[b] Beijing Institute of Electronic System Engineering, Beijing 100039, China
[c] Key Laboratory of Microgravity, Institute of Mechanics, Chinese Academy of Sciences, Beijing 100190, China
[d] School of Engineering Sciences, University of Chinese Academy of Sciences, Beijing 100049, China

Received 14 March 2022; revised 7 April 2022; accepted 13 May 2022
Available online 11 September 2022

KEYWORDS

Asymmetric performance;
Direct thrust test;
Ionic liquid electrospray thruster;
Time of flight mass spectrometry;
Torsional thrust stand

Abstract In order to meet the demand of CubeSats for low power and high-performance micro-propulsion system, a porous ionic liquid electrospray thruster prototype is developed in this study. 10 × 10 conical emitter arrays are fabricated on an area of 3.24 cm^2 by computer numerical control machining technology. The propellant is 1-ethyl-3-methylimidazolium tetrafluoroborate. The overall dimension of the assembled prototype is 3 cm × 3 cm × 1 cm, with a total weight of about 15 g (with propellant). The performance of this prototype is tested under vacuum. The results show that it can work in the voltage range of ±2.0 kV to ±3.0 kV, and the maximum emission current and input power are about 355 μA and 1.12 W. Time of Flight (TOF) mass spectrometry results show that cationic monomers and dimers dominate the beam in positive mode, while a higher proportion of higher-order solvated ion clusters in negative mode. The maximum specific impulse is 2992 s in positive mode and 849 s in negative mode. The thrust is measured in two methods: one is calculated by TOF results and the other is directly measured by high-precision torsional thrust stand. The thrust (T) obtained by these two methods conforms to a certain scaling law with respect to the emission current (I_{em}) and the applied voltage (V_{app}), following the scale of $T \sim I_{em}V_{app}^{0.5}$, and the thrust range is from 2.1 μN to 42.6 μN. Many thruster performance parameters are significantly different in positive and negative modes. We speculate that due to the higher solvation energy of the anion, more solvated ion clusters are formed rather than pure ions under the same electric field. It may help to improve thruster performance if porous materials with smaller pore sizes are used as reservoirs.

* Corresponding author.
E-mail address: bitwzw@bit.edu.cn (Z. WU).
Peer review under responsibility of Editorial Committee of CJA.

Production and hosting by Elsevier

https://doi.org/10.1016/j.cja.2022.09.007

Although there are still many problems, most of the performance parameters of ILET-3 are good, which can theoretically meet the requirements of CubeSats for micro-propulsion system.

1. Introduction

CubeSats is one of the hot spots in the field of space research.[1] Because of its advantages of small size, light weight, low cost, flexible launch mode, short development cycle and high functional density, CubeSats plays an important role in scientific research, national defense and commercial fields, and has broad application prospects.[2–6] As CubeSats needs to perform more demanding space tasks, such as long-term orbital position maintenance, specific orbit transfer, and end-of-life deorbit, the need for propulsion systems is becoming more and more urgent.[7–11] However, due to the limitations of size and power, most of CubeSats do not carry propulsion devices, so it is of great significance to develop the micro-propulsion technology suitable for CubeSats[12].

Ionic Liquid Electrospray Thruster (ILET) is a kind of thruster based on electrospray principle, in which a liquid propellant at the tip of the emitter generates charged particles that are accelerated by an electric field.[13] ILETs generally produce a thrust of the magnitude of micronewtons.[14,15] The thruster has the advantages of small size, low power, high specific impulse, high efficiency and continuously adjustable thrust, which makes it one of the best candidate thrusters for CubeSats. In recent years, ILET has become a hot research topic[16–20].

Thrust is one of the important performance parameters of thruster, which can be obtained directly by torsional thrust stand and mass balance, and can be obtained indirectly by Time of Flight (TOF) mass spectrometry. Every measurement method has their own features. Thrust estimation from TOF is a common method used by most researchers.[21–25] The thrust obtained by this method is often greater than the actual thrust because the effects of angular dispersion, transmission and energy efficiency are ignored.[26] However, with the help of the TOF mass spectrometry, the composition of charged particles in beam can be obtained. High-precision mass balance is a method to directly measure the thrust of thruster.[14,27,28] The characteristic of this method is that the thrust and mass flow of propellant can be obtained at the same time. Huang et al.[14] directly measured the thrust and mass flow rate of the thruster with a mass balance, and then obtained other performance parameters of the thruster. Although this method is easy to implement, a measurement method with a faster response to the thrust is still desirable.

Utilizing the torsional thrust stand, high-precision measurement results can be obtained with fast response.[29] This method can measure the thrust at the level of μN or even sub-μN. Torsional thrust stand requires professional and systematic design, so only a few institutions can carry out relevant tests.[30,31] Krejci et al.[31] used a series of methods to characterize the performance of a passively fed electrospray microthruster prepared by laser ablation, including two independent thrust tests (magnetically levitated balance and torsional thrust stand). Directly measured thrust using the torsional thrust stand is compared to the calculated thrust using TOF data, which is modified according to the angular and energy efficiency. The results showed that the thrust obtained by the two methods was close to each other in a certain range. Recently, Natisin et al.[26,30] used a single-axis torsional thrust stand to measure the thrust of a porous-media electrospray thruster manufactured by the Computerized Numerical Control (CNC) machine. At the maximum input power ~1.3 W, the maximum thrust measured in the positive mode and the negative mode is 41 μN and 37 μN, respectively. Passively ionic liquid electrospray thruster has been studied in detail by many researchers. However, for the thruster prototype processed by CNC machine, the thrust performance calculated by TOF and the thrust measured directly by torsional thrust stand have not been compared comprehensively.

On the other side, the phenomenon of asymmetry current has been found in many studies, and the degree is more or less[32–34]. One characteristic of ionic liquid electrospray thruster is that it can emit cations or anions, which is expected to realize the self-neutralization of beam by periodically changing the polarity of applied voltage.[28,35] This asymmetry of thruster performance in positive and negative modes may complicate the modulation mode of beam self-neutralization. Therefore, it is necessary to study this asymmetry.

Therefore, a prototype of porous ionic liquid electrospray thruster is developed in this study. The porous glass emitter is processed by low-cost and fast iterative CNC machine method, the extractor is manufactured by mask chemical etching, and other parts of the thruster are processed by conventional mechanical methods. The ion species composition and angular distributions of the thruster beam are characterized by using a self-built TOF experimental device and a linear motion platform. In addition, the thrust of the prototype is directly measured by a torsional thrust stand developed by the Institute of Mechanics, Chinese Academy of Sciences. Finally, the performance of the thruster is discussed, focusing on the comparison of two thrust measurement results and the asymmetry of thruster performance under positive and negative polarity.

2. Manufacturing process of thruster prototype

In this study, a prototype of porous ionic liquid electrospray thruster (named as ILET-3) is designed. The overall structure is shown in Fig. 1 and its external size is 30 mm × 30 mm × 10 mm. The thruster prototype consists of extractor electrode, upper enclosure, emitter, propellant reservoir layer, lower enclosure and distal electrode, as shown in the order from left to right in Fig. 1(a). The thruster prototype after assembly is shown in Fig. 1(b).

The emitter is made of porous borosilicate glass material (G5, pore size is about 2–4 μm) manufactured by CNC machining method, and total 100 conical emitter tip arrays (10 × 10) are on an area of 3.24 cm^2. The bottom radius

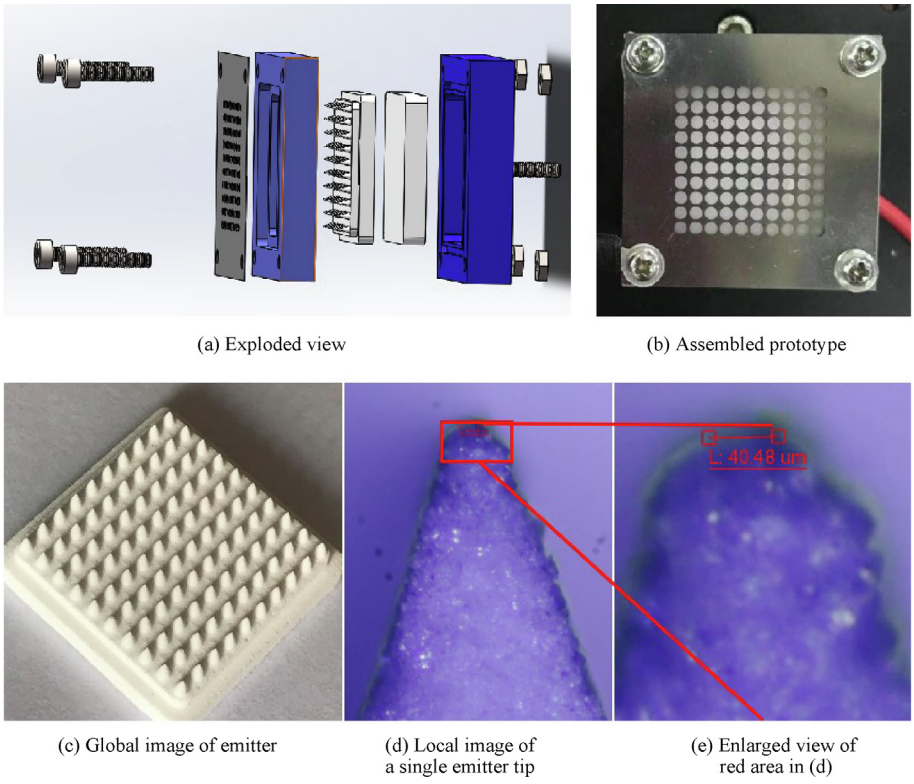

(a) Exploded view (b) Assembled prototype

(c) Global image of emitter (d) Local image of a single emitter tip (e) Enlarged view of red area in (d)

Fig. 1 Thruster prototype of ILET-3.

and height of each conical emitter are 0.5 mm and 1.5 mm respectively, so the half angle of the cone is about 18.4°. The emitter tip structure is observed with an optical microscope, as shown in Fig. 1, and the radius of the cone tip is about 20 μm. The distance between cones is 1.8 mm. The overall shape of the emitter and the optical image of each tip are shown in Figs. 1(c)–1(e). The propellant reservoir layer is also made of porous borosilicate glass material (G2, pore size is about 30–50 μm) by CNC method. The size is 20 mm × 20 mm × 3 mm. It is connected to the power supply through a distal electrode under the reservoir layer. The research results of Courtney and Shea[36] showed that the difference of pore size between the reservoir and the emitter layer produced a Laplace pressure, so that the propellant can be continuously supplied from the reservoir to the emitter layer.

The extractor electrode is made of stainless steel by mask chemical etching method. The aperture of the extractor is 1.5 mm in diameter and the spacing is 1.8 mm. The thickness of the extractor electrode is 0.1 mm. The upper and lower enclosures are made of Polyether Ether Ketone (PEEK) material and manufactured by conventional machining method. Attention should be paid to the groove depth of the upper enclosure to control the distance between the tip of the emitter and the extractor required for the design. In ILET-3, this distance is 0.1 mm. The thruster prototype is assembled with metal or alumina ceramic screw mounting. All parts of the thruster prototype are assembled with ceramic screws, and the gap between the upper and lower enclosures is sealed by rubber rings.

In this study, 1-ethyl-3-methylimidazolium tetrafluoroborate (EMI-BF_4) is used as propellant. It needs to be degassed in a vacuum chamber with a pressure of 10^{-2} Pa for more than 12 h before loading it into the reservoir and emitter. The loading volume of propellant is about 1 mL. The total mass of the thruster prototype after propellant EMI-BF_4 loading is about 15 g. After loading the propellant, the thruster is assembled as quickly as possible and transferred to the vacuum chamber, and then the test is started.

3. Experimental apparatus and methods

In order to simulate the operation of ILET-3 in the space environment, the performance of the thruster prototype was tested in the vacuum chamber, including the following four parts: (A) general ignition test, current measurement and beam images at different voltages; (B) time of flight mass spectrometry; (C) beam angular distributions; (D) direct thrust test. The first three tests were carried out in the vacuum chamber in Jet Propulsion Laboratory, Beijing Institute of Technology. The vacuum system consists of one cylindrical vacuum chamber (0.5 m in diameter and 0.8 m in length), two rotary vane mechanical vacuum pumps, one molecular pump, cooling water tank and control box. The pressure in the vacuum chamber during the tests was about 5×10^{-3} Pa. The direct thrust test was carried out in the vacuum chamber of the Key Laboratory of Microgravity, Institute of Mechanics, Chinese Academy of Sciences. The pressure during the test was 1×10^{-3} Pa.

3.1. General ignition test, current measurement and beam images

A positive DC high-voltage power and a negative DC high-voltage power (DW-N303/DW-P303) were connected to a pulse generator (PVX-4110, DEI), which can quickly generate high-voltage waveforms up to 10 kV. The frequency and duty

cycle of the output voltage waveform of the pulse generator were controlled by a function generator, and the amplitude of the output voltage is controlled by two DC high-voltage power supplies. The output high voltage was connected to the emitter through a 1 MΩ sampling resistor. The extractor electrode was grounded after connecting a 100 kΩ sampling resistor. The above method can not only protect the circuit, but also obtain the current by measuring the voltage drop on the sampling resistance.

Three types of currents were measured in this study. The first was the current in the emitter circuit (named as total current, I_t), it was obtained by measuring the voltage across the 1 MΩ sampling resistor with a multimeter (OWON B35 +), and the data are transmitted to the computer by Bluetooth. The second was the current in the extractor circuit (named as intercepted current, I_{ex}), and it was obtained by using a passive voltage probe (Tektronix TPP0250) to measure the voltage across the 100 kΩ sampling resistor, and recorded by the oscilloscope (Tektronix MDO3014). The third was the emission current, I_{em}. Based on the following Eq. (1) of the above three currents, I_{em} can be calculated:

$$I_t = I_{ex} + I_{em} \quad (1)$$

Before the current measurement, general ignition test was carried out according to the following steps to determine the working voltage range of the prototype. When the prototype was installed in the vacuum chamber and the pressure met the requirements of the experiment, we turned on the power supply and raised the voltage of the emitter in the way of alternating positive and negative polarity with each step of 100 V. When the intercepted current was greater than 0.5 μA, the emitter was considered to start working and the voltage at this time was taken as the onset voltage. The voltage was raised until the electrode was abnormally discharged, which was determined as the maximum working voltage of the thruster prototype. Then we reduced the voltage with the same parameters. This process was repeated 10 times, the emission state of the thruster prototype was stable, and then the current and voltage were measured and recorded. The above three currents were measured at 100 V intervals in the working voltage range, and this measurement was repeated three times.

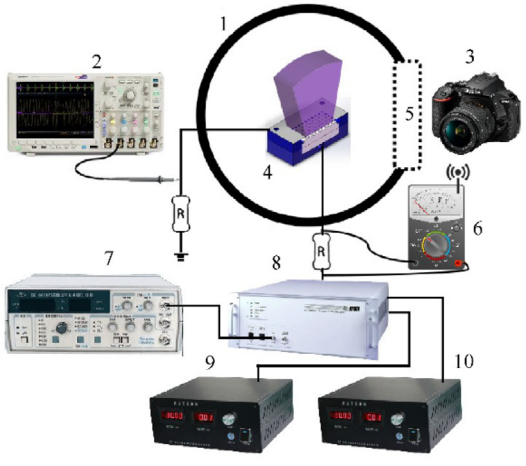

1—Vacuum chamber; 2—Oscilloscope; 3—Camera; 4—Prototype;
5—Glass porthole; 6—Multimeter; 7—Function generator ;
8—Pulse generator; 9—Positive high voltage power;
10—Negative high voltage power

Fig. 2 Schematic diagram of experimental setup for measuring current and capturing beam.

During the ignition process of the thruster prototype, the beam images under different voltages were taken and recorded by the camera. In this process, the side or downstream of the thruster was facing the center of the glass porthole on the vacuum chamber. The digital camera (Nikon D5600) was installed outside the porthole of the vacuum chamber. After adjusting the focus of the lens and setting the camera parameters, the beam images can be captured. The schematic diagram of the experimental setup for measuring current and capturing beam is shown in Fig. 2.

3.2. Measurement method of beam angular distributions

A small self-built Faraday cup was installed on a linear motion platform to measure the beam angular distribution of the thruster prototype (Fig. 3(a)). The area of the current collector in the Faraday cup is 0.33 cm^2, and there is a −40 V grid in front of the collector to suppress secondary electron. The current was obtained by measuring the voltage across the 100 kΩ sampling resistance as the intercepted current measurement method in Section 3.1. The onset voltage of the stepping motor is used as the trigger signal to record the collector current on the oscilloscope. Firstly, the current at different times is obtained on the oscilloscope. Since the Faraday cup moves at a constant speed of 4 cm/s, the current at different positions can be obtained. The distance between the Faraday cup and the emitter is 7.5 cm. The length of the linear motion platform is 20 cm and the thruster is aligned with its center. According to the above geometric relationship, the current at different angles, that is, the angular distribution of the current, can be calculated. Assuming that the spatial current distribution of all single emitters is the same, taking the emitter on the outermost side of the thruster as an example, the maximum angle that can be measured by the system is arctan [(10–0.9)/7.5] = 50.5° (Fig. 3(b)). It should be noted that the current in the middle area is formed by the superposition of the current of multiple single point emitters, so the current angular distribution of each single point emitter cannot be obtained, and the current angular distribution finally obtained is that of the whole thruster. Each test was repeated 6 times to reduce the error.

3.3. Measurement method of TOF

TOF is an important method to characterize the performance of ILET and the composition of charged particles in beam. Its basic principle is that after the beam is interrupted, the accelerated charged particles fly a certain distance in the non-electric field area and reach the collector electrode. Due to the different speeds of charged particles with different specific charge accelerated by the same electrostatic field, the time to reach the collector electrode is also different, and the current signal will gradually decrease to zero, as shown in Fig. 4. There are two ways to interrupt the beam. One is to set a group of electrostatic gate electrodes downstream of the thruster. When a fast-pulsed high voltage is applied to the electrostatic gate, the plume is interrupted. This method is used by most researchers,[27,37] but the use of multilayer electrostatic gate electrodes will reduce the transparency of the beam and the

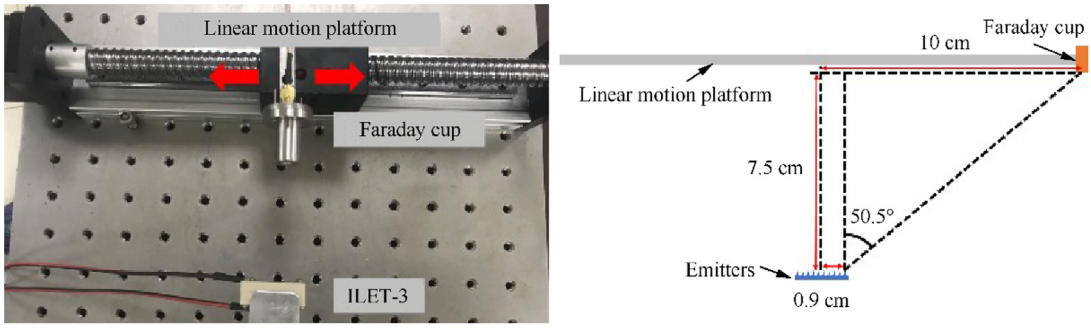

(a) Experimental setup of beam angular distribution (b) Schematic diagram of angular distribution calculation

Fig. 3 Experimental setup and schematic diagram of beam angular distribution.

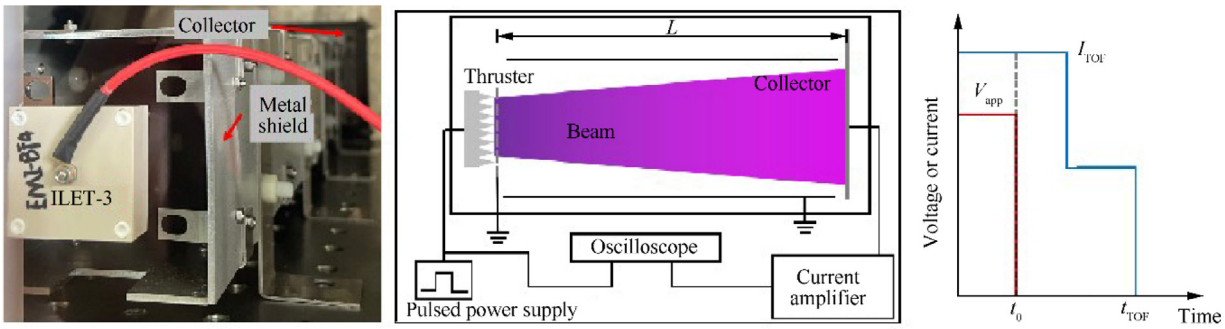

(a) Experimental setup of TOF (b) Schematic diagram of TOF (c) Ideal voltage and current signal curve of TOF

Fig. 4 Experimental setup and schematic diagram related to TOF test.

detected current signal. Another method is to turn off the high voltage on the emitter directly and the emission is considered to stop instantaneously.[38,39] The latter method is used in this study.

Specifically, the thruster prototype and the stainless-steel collector were placed horizontally and center-aligned, and fixed on the optical platform. The distance (L) between the emitter and the TOF collector was 0.43 m. The pulse signal generator is used to generate a 10 Hz square wave with a duty cycle of 50 %, and the voltage output is controlled by the bipolar pulse generator. The emitter voltage was detected by a high voltage differential probe (Tektronix THDP0100) and recorded by an oscilloscope (Tektronix MDO3014). The fast rising or falling edge of the applied emission voltage (V_{app}) was set as the trigger signal, which is regarded as the TOF initial time t_0, and the time when the current signal (I_{TOF}) is reduced to 0 μA is t_{TOF}. The current signal of the collector is transmitted to the oscilloscope for display and record through the current amplifier (FEMTO DHPC-100). The oscilloscope was set to 64 times averaging to reduce random error. In order to reduce the electromagnetic interference caused by fast pulse high voltage, BNC coaxial cable was used and a metal shield was placed on the path of the beam. The experimental setup and schematic diagram of TOF test are shown in Figs. 4(a) and 4(b).

3.4. Directly measurement method of thrust

The torsional thrust stand system used in this research is designed and developed in the Key Laboratory of Microgravity, Institute of Mechanics, Chinese Academy of Sciences. The high-precision capacitive displacement sensor is used as the torsion angular displacement sensing device in this system. A high-precision electronic balance is used to calibrate the standard force generated by the electrostatic comb, then the torque pendulum is calibrated by the electrostatic comb, and the relationship between the thrust and angular displacement is obtained finally. The thrust resolution of the system is 0.025 μN, the thrust measurement range is 0.025–400 μN, the measurement error is 0.98 %, and the power spectral density of background noise is better than 0.1 $\mu N/Hz^{1/2}$ (10 mHz – 1 Hz).[29] A metal liquid box is placed directly above the pivot so as to bridge the electric wire, which aids in eliminating the torque interference induced by the wire during the actual thrust test. This system can realize steady and dynamic micro thrust test and cover the thrust range of ILET. The schematic diagram of the total torsional thrust stand system is shown in Fig. 5(a)[29].

In the direct thrust test experiment, ILET-3 was fixed on a certain moment arm of the torsional thrust stand, as shown in Fig. 5(b). The thrust axis was aligned with the center of the moment arm, and then the counterweight was added and levelled. The line layout was optimized and the coaxial high-voltage cable was used to reduce the electrostatic force. It was found that the electrostatic force was less than 0.1 μN when the voltage is 3000 V. The stand with ILET-3 prototype was placed into the vacuum chamber. When the pressure reached below 1×10^{-3} Pa, the thrust stand was calibrated first, and then the thrust can be measured. The thrust was

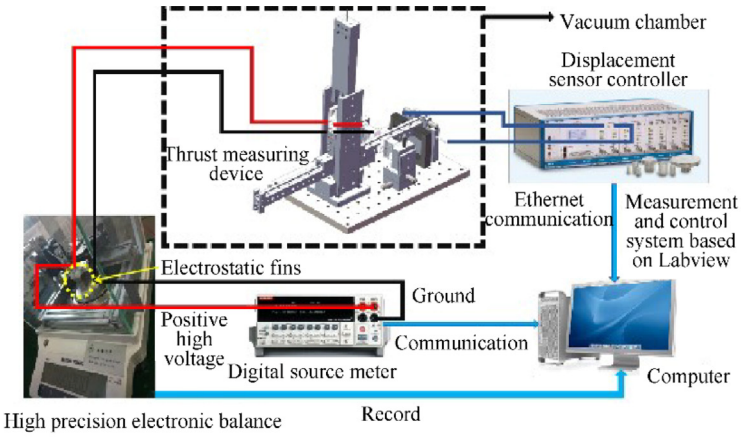

(a) Schematic diagram of torsional thrust stand system[29]

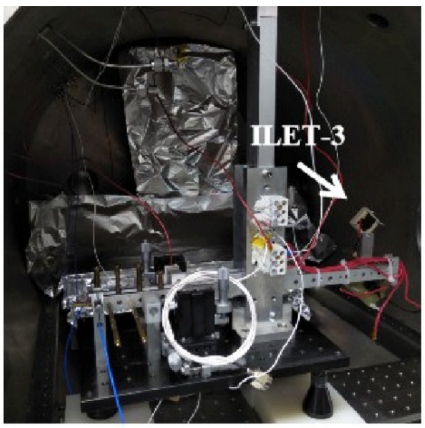

(b) ILET-3 and torsional thrust stand in vacuum chamber

Fig. 5 Schematic diagram and experimental setup related to direct thrust test.

finally recorded in the computer, and the current and voltage of the thruster were measured according to the same method in Section 3.1.

4. Results

4.1. Emission characteristics

The emission characteristics test is the general experiment to characterize the performance of the thruster. After the assembly of the thruster, the emission characteristics are tested at different voltages. Because ILET can work at both positive and negative voltages, the thruster ignition test is carried out in alternating positive and negative voltages. The general emission characteristics of the thruster are studied by capturing the beam images and measuring the current of the thruster under different voltages. The side view and front view of beam images of ILET-3 operating in the vacuum chamber are shown in Fig. 6. It can be seen that the beam of ILET-3 prototype is obvious under both positive and negative voltages, and the brightness of the beam increases with the increase of voltage. The side view of the beam images under positive and negative voltages are similar, but the front view of the beam images are different. The color of the beam is blue under positive voltage and purple under negative voltage, and the beam is more uniform under negative voltage. It is speculated that the performance of the prototype under positive and negative voltages may be different, which is discussed in detail in Section 5.

The above results show that ILET-3 can work under both positive and negative voltages, and the emission current increases with the increase of voltage. Too high voltage will cause abnormal discharge and damage the thruster. For example, when the voltage is higher than 3 kV, there will be abnormal discharge between the emitter and the extractor electrode (not shown in the image). Therefore, it is determined that the working voltage range of the ILET-3 prototype is ±2 - ±3 kV.

The general ignition test is operated in positive and negative alternating mode. The typical applied voltage and current curves are shown in Fig. 7(a). After the increase and decrease voltage operations are repeated for 10 times, alternating positive and negative voltages increasing from ±2 kV to ±3 kV (increase the amplitude by 100 V each time) are applied to the emitter, and the current–voltage characteristic curve of ILET-3 is measured. Take the average value of the three measurement results, and the current-voltage curve with error bar is shown in Fig. 7(b). The input power obtained by multiplying the applied voltage by the total current is also shown in Fig. 7 (b).

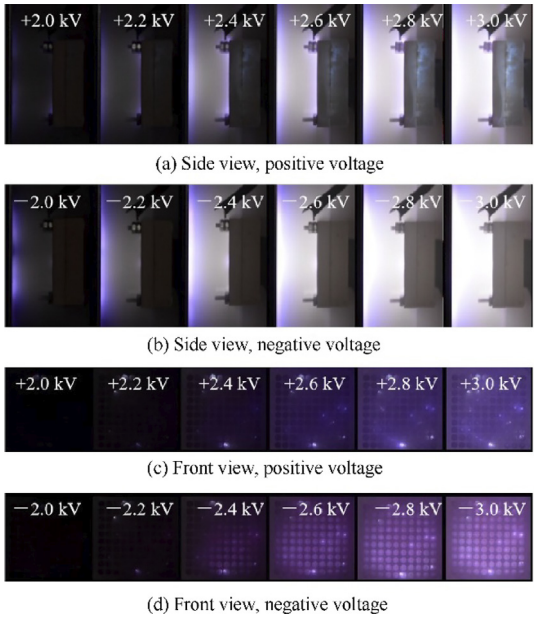

(a) Side view, positive voltage

(b) Side view, negative voltage

(c) Front view, positive voltage

(d) Front view, negative voltage

Fig. 6 Beam images under positive and negative voltages (ISO2000, exposure time is 5 s).

It can be seen that the onset voltage of the prototype ILET-3 is about ±2 kV. According to the existing research results,[33,40] the onset voltage (V_{on}) of porous electrospray thruster can be estimated by

$$V_{on} = \sqrt{\frac{\pi\gamma R_e}{4\varepsilon_0}}\sqrt{\frac{R_e}{r_p}}\ln\left(\frac{4d}{R_e}\right) \tag{2}$$

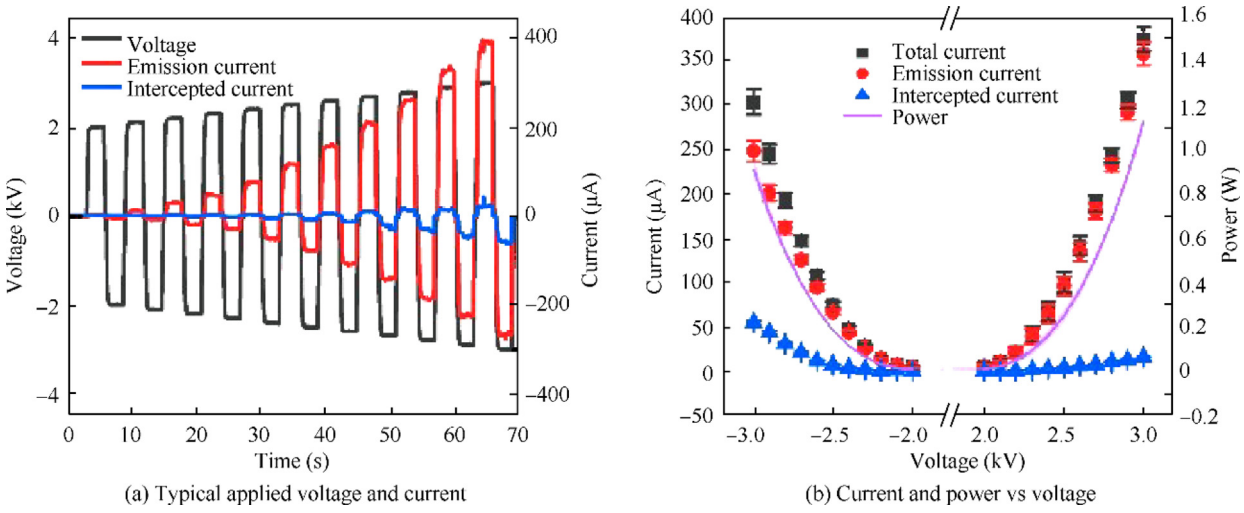

Fig. 7 Typical electrical characteristics of ILET-3 prototype.

where γ is the surface tension coefficient of EMI-BF_4, R_e is the radius of the emitter tip, ε_0 is the vacuum permittivity, r_p is the pore radius of the porous emitter, and d is the distance between the emitter tip and the extractor. By substituting the parameters of ILET-3 into Eq. (2), the onset voltage can be calculated to be about 2035 V, which is consistent with the onset voltage measured by experiments.

Under both positive and negative voltage modes, the total current, intercepted current and emission current increase with the increase of applied voltage, and the input power also increases. However, the currents of the two modes under the same voltage value are different, which shows an asymmetric current-voltage curve. The maximum total current and emission current in positive mode are about 375 μA and 355 μA, respectively, while those in negative mode are 300 μA and 250 μA, respectively. The intercepted current is also different between the two modes. The maximum intercepted current in positive mode is 16 μA. In negative mode, it is up to 55 μA. Due to the difference of total current, the input power is also different. The input power range of positive mode is 0.01–1.12 W and that of negative mode is 0.01–0.91 W. Asymmetric current-voltage curves have also been found in other studies,[24-28,41] which will be discussed in Section 5.2.

4.2. Beam angular distributions

Fig. 8 shows the beam angular distributions of ILET-3, where Figs. 8(a) and 8(b) are the angular distributions of the emission current detected by the Faraday cup at different voltages, and Figs. 8(c) and 8(d) are the normalized curves by their respective maximum current. The results show that, under the same voltage value, the emission current detected in positive mode is higher than that in negative mode, which is consistent with the results of current measurement in Section 4.1. Except ±2.2 kV, the beam angular distributions in both modes are symmetrical, and the center is near 0°. The reason may be that not all emitters are ignited when the applied voltage is ±2.2 kV, as shown in Figs. 6(c) and 6(d).

The effective divergence half angle (θ_{eff}) is defined as the angle of a virtual point emitter produces the same thrust.[27] It can be calculated according to

$$\cos\theta_{\text{eff}} = \int_{-\theta_{\max}}^{+\theta_{\max}} f(\theta)\cos\theta \mathrm{d}\theta \tag{3}$$

where $f(\theta)$ is the current angular distribution function normalized by the total emission current (i.e. the total area of the bean current angular distribution).

Since the beam angular distribution under each applied voltage is similar, θ_{eff} is finally calculated by using the current data when the applied voltage is ±3 kV. It can be calculated that θ_{eff} is 18.2° and 18.6° at 3 kV and –3 kV, respectively, so we take the average value of 18.4° as the effective divergence half angle of ILET-3. This value is similar to or smaller than that reported by other researchers,[22,30,42] indicating higher angular efficiency of ILET-3 prototype. The effective divergence half angle is related to the aperture of the extractor and the distance between the extractor and the emitter. A small aperture and a large distance are conducive to reducing the effective divergence half angle, but will increase the intercepted current, which may be one of the reasons for the large intercepted current of ILET-3.

4.3. TOF

A typical TOF signal is shown in Fig. 9, which is collected by the TOF test system described in Section 3.3 when the thruster is operating at +2.6 kV. The sharp fluctuation of the original current data at time 0 μs is due to the electromagnetic interference caused by the pulse voltage falling to zero in hundreds of nanoseconds. It can be controlled less than 3 μs through the shielding treatment of the experimental system. It is calculated that the fastest ion in beam reaches the collector after 5 μs according to the flight distance and theoretical speed. Therefore, this fluctuation has no effect on the diagnosis of TOF current. A smooth curve can be obtained after the original current data are processed by Fast Fourier Transform (FFT) filter (window point is 2500). After the applied voltage is turned off, the detected current decreases to zero in about 11 μs. When the current decreases to 0 μA, overshoot occurs and then returns to zero at 30 μs. This phenomenon also appeared in the experiments of other researchers,[43,44] probably due to the influence of secondary electrons. The TOF test system needs to be fur-

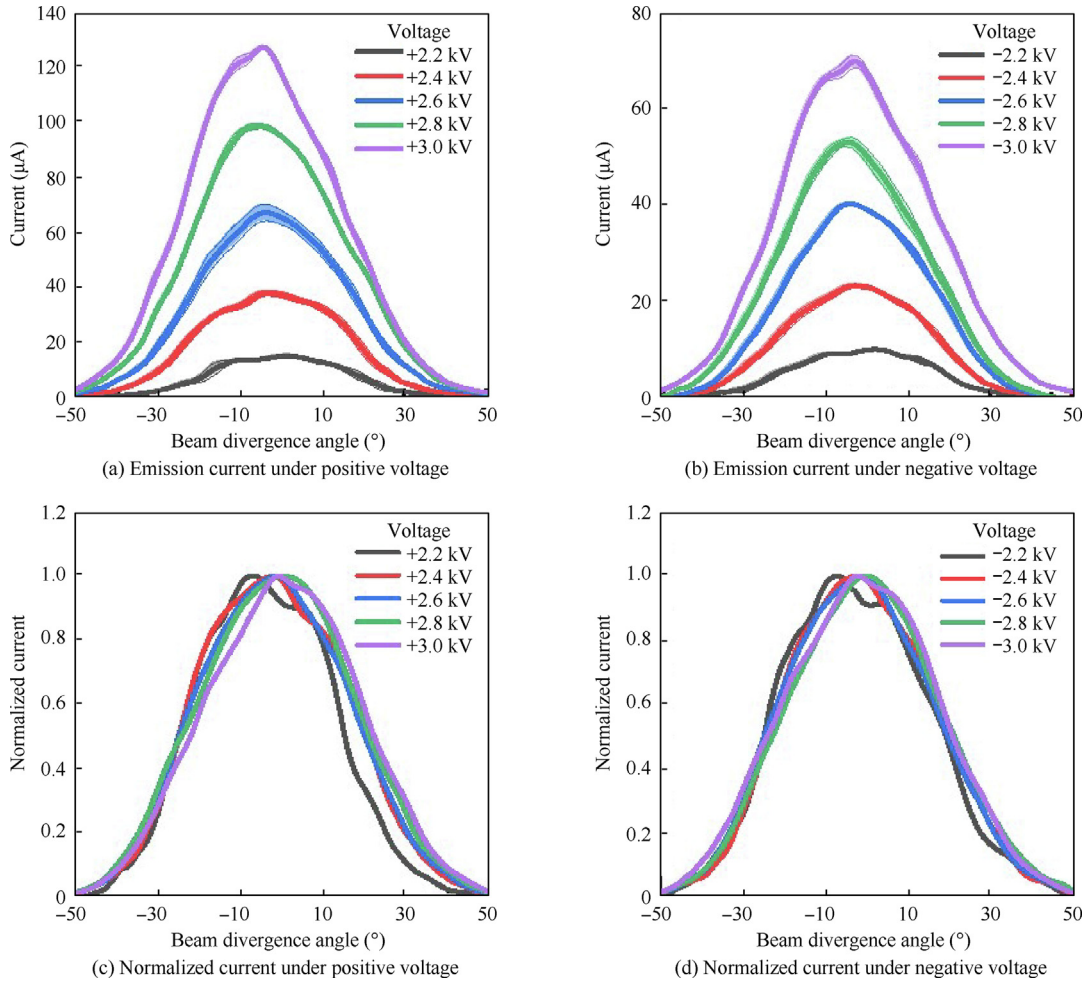

Fig. 8 Beam divergence angle distributions of ILET-3 under positive and negative voltages.

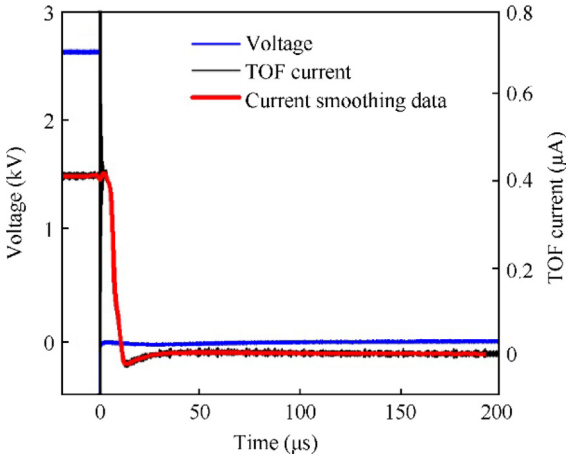

Fig. 9 A typical TOF signal and processing method.

ther improved, but we believe that this phenomenon has little effect on the analysis of thruster performance using TOF curve.

In the thruster with ionic liquid EMI-BF_4 as propellant, it is generally considered that there are pure ions and solvated ion clusters in the beam. In the positive mode, it is mainly $(EMI\text{-}BF_4)_nEMI^+$ (n = 0,1,2,...), and in the negative mode, it is mainly $(EMI\text{-}BF_4)_nBF_4^-$ (n = 0,1,2,...). The atomic masses of these ions are shown in Table 1.

In the experiment, ten sets of data of positive and negative modes from ±2.2 kV to ±3.0 kV are tested, as shown in Fig. 10(a). In order to compare the ion species composition of the beam under different voltages, the time axis can be converted into the mass axis according to Eq. (4) and Eq. (5), and the TOF current under different voltages can be normalized, as shown in Fig. 10(b). The auxiliary lines are the theoretical mass of the labeled ion or ion cluster.

$$\frac{1}{2}mv^2 = qV_{\text{app}} \tag{4}$$

$$v = \frac{L}{t} \tag{5}$$

where v is the velocity of the ions in the beam, m is the mass of ions, q is the charge of ions (here it is regarded as elementary charge), V_{app} is the voltage applied on the emitter, and t is the flight time of ions.

It can be seen from Fig. 10(a) that the TOF current curve is not an ideal step decline, but with a certain slope, which may be due to the influence of the beam angle and the decomposi-

Table 1 Possible ion species and their atomic mass in beam.

Ion	n	Atomic mass (Da)
$(EMI\text{-}BF_4)_nEMI^+$	0	111.2
	1	309.1
	2	507.1
$(EMI\text{-}BF_4)\ _nBF_4^-$	0	86.8
	1	284.8
	2	482.8

tion of droplets or ion clusters in the beam during acceleration. There are abnormal distortions in the TOF curves obtained from the experiment, just like the results of other researchers,[15,25,27,31,45] Gamero-Castaño[45] believed that the abnormal distortions were caused by capacitive coupling between the emitter and the collector electrodes.

Fig. 10(b) shows that the ion species composition in the beam of ILET-3 is significantly different in positive and negative modes. In the positive mode, there are only two ion species in the beam, which are pure ion EMI^+ and solvated ion cluster $(EMI\text{-}BF_4)\ EMI^+$. But in the negative mode, the ion species composition in the beam is very complex. The mass of the largest solvated ion cluster is more than 10000 Da, and the proportion of pure ion species also increases with the increase of applied voltage. For example, the proportion of pure ion BF_4^- increases from 10 % at −2.2 kV to 35 % at −3.0 kV. The approximate ion species composition of the beam in positive and negative modes is summarized in Table 2.

Besides the ion species composition of the beam, the thrust, mass flow rate, specific impulse and polydisperse efficiency of the thruster can be calculated according to Eqs. (6)–(9), and the results are listed in Table 3.

$$T_{\mathrm{TOF}} = \frac{I_{\mathrm{em}}}{I_{\mathrm{TOF}}} \int_{t_0}^{t_{\mathrm{TOF}}} \frac{2V_{\mathrm{app}}}{L} I(t)\mathrm{d}t \tag{6}$$

where T_{TOF} is the calculated thrust by TOF data, I_{TOF} is the initial current of TOF curve and $I(t)$ is the TOF current curve.

$$\dot{m}_{\mathrm{TOF}} = \frac{I_{\mathrm{em}}}{I_{\mathrm{TOF}}} \int_{t_0}^{t_{\mathrm{TOF}}} \frac{4V_{\mathrm{app}}}{L^2} I(t)t\mathrm{d}t \tag{7}$$

where $\dot{m}_{\mathrm{TOF}}$ is the mass flow rate calculated by the TOF data.

$$I_{\mathrm{sp}} = \frac{T_{\mathrm{TOF}}}{\dot{m}_{\mathrm{TOF}} g} \tag{8}$$

where I_{sp} is the specific impulse and g is the gravitational acceleration of the earth.

$$\eta_{\mathrm{ploy}} = \frac{T_{\mathrm{TOF}}^2/(2\dot{m}_{\mathrm{TOF}})}{V_{\mathrm{app}} I_{\mathrm{em}}} \tag{9}$$

where η_{ploy} is the polydisperse efficiency of thruster.

It should be noted that the above thrust (T_{TOF}) and mass flow rate ($\dot{m}_{\mathrm{TOF}}$) are the total thrust and total mass flow of the thruster calculated according to the ratio of I_{TOF} and I_{em}, by assuming that the beam of the thruster is uniform and the composition and energy of ion species in the beam are independent of the spatial distribution. The polydisperse efficiency is the loss due to accelerating ions of varying specific charge through the acceleration region, not the total efficiency of the thruster. It can be seen that in both positive and negative modes, with the increase of applied voltage, the mass flow, thrust and specific impulse increase, while the polydispersive

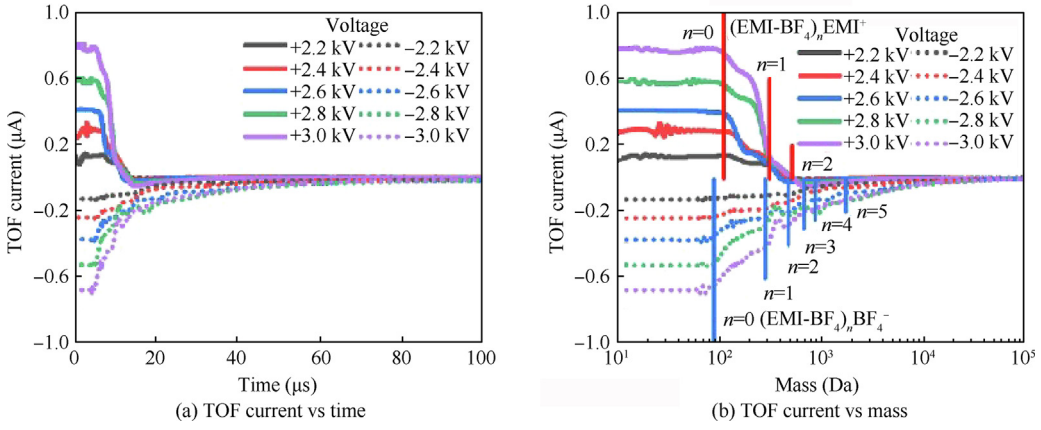

Fig. 10 Variation of TOF current with time and mass under different voltages.

Table 2 Approximate ion species composition of beam in positive and negative modes.

V_{app} (kV)	$(EMI\text{-}BF_4)_nEMI^+$ composition (%)		$(EMI\text{-}BF_4)_nBF_4^-$ composition (%)		
	$n = 0$	$n = 1$	$n = 0$	$n = 1$	$n \geq 2$
2.2	30	70	10	10	80
2.4	45	55	20	20	60
2.6	60	40	35	15	50
2.8	20	80	40	20	40
3.0	20	80	35	25	40

Table 3 Performance of ILET-3 calculated by TOF data.

V_{app}(kV)	I_{em}(μA)	I_{TOF}(μA)	$\dot{m}_{TOF}$ (μg/s)	T_{TOF}(μN)	I_{sp}(s)	η_{ploy}
+2.2	21.76	0.134	0.12	2.58	2118	0.559
+2.4	64.56	0.290	0.28	7.04	2536	0.565
+2.6	134.93	0.410	0.53	14.15	2733	0.540
+2.8	232.58	0.584	0.88	24.77	2872	0.535
+3.0	357.79	0.781	1.21	35.48	2992	0.485
−2.2	−13.87	−0.124	0.72	4.38	620	0.436
−2.4	−44.12	−0.237	1.66	12.00	739	0.410
−2.6	−95.31	−0.365	3.41	23.89	715	0.338
−2.8	−161.62	−0.519	4.11	34.21	849	0.315
−3.0	−248.29	−0.669	5.75	46.47	825	0.252

efficiency decreases slightly. It shows that in the porous electrospray thruster, the flow rate of the propellant is not a constant, but positively correlated with the voltage. Therefore, this type of thruster can adjust the thrust performance by changing the applied voltage. The thrust performance parameters of positive and negative modes are quite different. The mass flow rate in positive mode is from 0.12 μg/s to 1.21 μg/s, and that in negative mode is from 0.72 μg/s to 5.75 μg/s. The mass flow rate in negative mode is several times that in positive mode. The thrust in positive mode is from 2.58 μN to 35.48 μN, and that in negative mode is from 4.38 μN to 46.47 μN. The thrust in negative mode is larger under the same voltage amplitude. The specific impulse in positive mode is more than 2000 s, up to 2992 s, while that in negative mode is only 620 s to 849 s. In terms of polydispersive efficiency, the maximum is 56.5 % in positive mode and 43.6 % in negative mode.

4.4. Thrust

The thrust of ILET-3 is measured by the torsional thrust stand system described in Section 3.4. The thrust and the total current under the positive and negative voltages of the continuous step are shown in Fig. 11. The applied voltage increases by 100 V every 9 s, from ±1.8 kV to ±3.0 kV. It can be seen that with the increase of applied voltage, the total current and thrust increase, also showing a step shape. The thrust can respond quickly within 1 s after voltage change in both modes. In the negative mode, the thrust is very stable at each applied voltage within the whole voltage range, while in the positive mode, the thrust is stable at low voltage, and pulse fluctuation occurs at high voltage (> +2.5 kV). It is speculated that this is related to more discharges between the emitter and the extractor,[46] as shown in Fig. 6(c).

The single thrust value of each voltage is obtained by averaging the thrust within the corresponding time range, and the average value of the three measurement results is taken as the final thrust. Finally, the thrust in positive mode is 2.3–31.8 μN, and in negative mode it is 2.1–42.6 μN, as shown in Fig. 12. Like the thrust calculated by TOF, under the same voltage amplitude, the thrust directly measured in positive mode is less than that in negative mode, which is related to the difference of ion species composition in the beam of these two modes.

5. Discussion

5.1. Comparison of two thrust measurement results

In this study, the thrust of ILET-3 prototype can be obtained in two methods, one is calculated by TOF results (indirect method), and the other is measured by high-precision torsional thrust stand (direct method). The two tests are carried out at different time and places using the same thruster prototype,

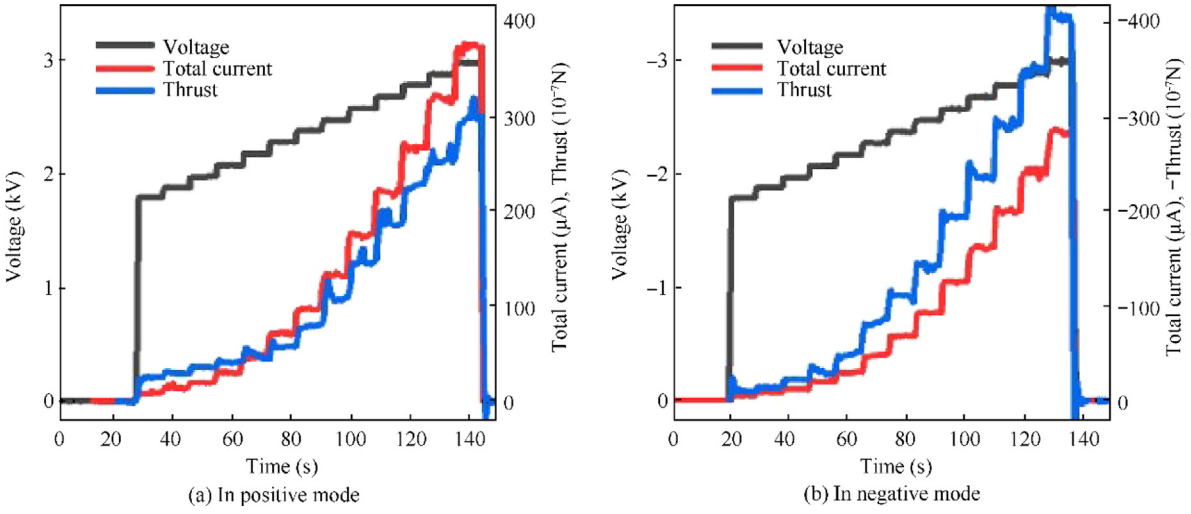

Fig. 11 Voltage, current and thrust in direct thrust test in positive mode and negative mode.

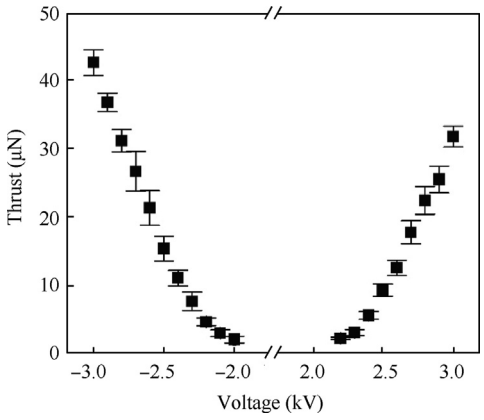

Fig. 12 Direct thrust test results of positive and negative modes.

and the emission current may be slightly different for the same applied voltage. Therefore, the relationship among thrust, applied voltage and emission current in each experiment is established according to $T \sim I_{em} V_{app}^{0.5}$, and the results of two thrust measurement methods are shown in Fig. 13. It should be noted that the thrust is calculated by TOF listed in Table 3 without considering the beam angular distribution, so we need to further multiply by a correction factor $\cos\theta_{eff}$ to obtain the thrust of the indirect method. According to the effective divergence half angle in Section 4.2, the correction factor of ILET-3 in this study is $\cos 18.4° \approx 0.95$. The data in Fig. 12 is used as the thrust of the direct method.

Fig. 13 shows that the thrust of the two methods is consistent in most cases, but shows different trends in the two voltage polarities. In positive mode, the relationship between thrust and $I_{em} V_{app}^{0.5}$ is approximately linear with a slope of 1648 μN/(A•V$^{0.5}$). However, it is nonlinear in negative mode, and the slopes of −2.0 kV to −2.6 kV and −2.7 kV to −3.0 kV are 4346 μN/(A•V$^{0.5}$) and 2330 μN/(A•V$^{0.5}$) respectively, obtained by piecewise fitting. Combined with the results of TOF in Section 4.3, it is considered that this difference is caused by the different ion species composition of the beam in the positive and negative modes. According to the conservation of momentum and energy, the thrust conforms to the following relationship:

$$T = I_{em}\sqrt{2V_{app}\langle m/q\rangle} \tag{10}$$

where $\langle m/q \rangle$ is the average mass-to-charge ratio of all ions in the beam.

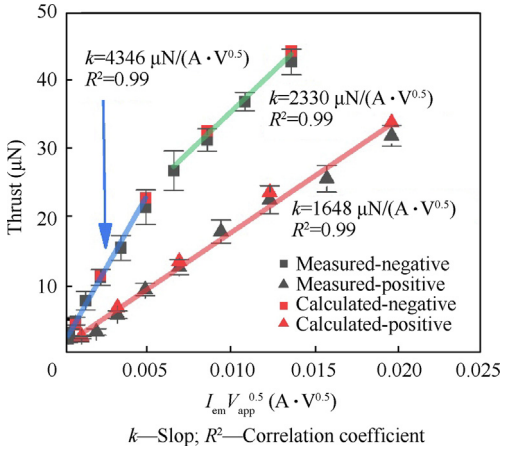

Fig. 13 Results of two thrust measurement methods (k is the slope and R is the correlation coefficient).

It is assumed that there are only pure ions, and m/q is a constant, so the thrust is linear with $I_{em} V_{app}^{0.5}$. But in fact, there are many kinds of ion species in the beam. As shown in Table 2, in the positive mode, there are only two kinds of ion species, and the change of component proportion has little effect on the average mass-to-charge ratio, so the relationship between thrust and $I_{em} V_{app}^{0.5}$ is approximately linear. In negative mode, the ion species composition of the beam is complex, and the average mass-to-charge ratio is greatly affected by the change of component proportion, so it is nonlinear. In addition, in positive mode, the beam is dominated by monomer and dimer, and average mass-to-charge ratio is small, so the slope of the fitting line is small. In negative mode, the proportion of polymer is large and the average mass-to-charge ratio is large, so the slope of the fitting line is large. However, with the increase of applied voltage, the proportion of light mass ions increases, so the slope tends to decrease.

Courtney et al.[27] compared the thrust calculated by TOF with the thrust measured by mass balance, but did not distinguish the positive and negative voltage polarity. The calculated total thrust was obtained according to a duty cycle coefficient under the two modes. They found that the thrust obtained by the two methods was close in most cases, but when 1-ethyl-3-methylimidazolium-bis(trifluoromethylsulfonyl) imide (EMI-Im) was used as propellant, the thrust of one thruster prototype (SRC-Im-1) was less consistent, which was attributed to inadequate thrust balancing. In fact, according to the results in Ref. 27, for two thrusters (SRC-Im-1 and SRC-Im-2) using EMI-Im as propellant, the thrust in positive mode is also less than that in negative mode (factor $\kappa \sim 0.7$), which is similar to our results. For the thruster (SRC-BF_4) using EMI-BF_4 as propellant, the thrust of positive and negative modes is close to each other and consistent with the thrust measured directly. From their TOF results,[27] it can be seen that there is a long tail in the TOF curves of SRC-Im-1 and SRC-Im-2 in negative mode, indicating the existence of heavy ion clusters, while there are fewer ion species in positive mode. There are fewer ion species in both positive and negative modes for SRC-BF_4. In addition, the thrust results of the two propellants are compared, and the fitting slopes of SRC-Im-1 and SRC-Im-2 are estimated to be about 3000 μN/(A•V$^{0.5}$), while it is about 1700 μN/(A•V$^{0.5}$) for SRC-BF_4.[27] These data are close to the two typical slopes in this study.

Krejci et al.[31] compared the thrust calculated by TOF under positive and negative polarity with the thrust measured by torsional thrust stand. The results also show that the thrust obtained by these two methods is consistent, and the thrust trend of positive and negative modes is also consistent. For EMI-BF_4 prototype, the TOF results show that there is a long tail in both positive and negative modes, and the proportion of ion species changes slightly, so the thrust of these two modes is close. However, due to the existence of heavy ion clusters, according to the applied voltage and emission current values in Ref.31, we estimate that the fitting slope is 2300 μN/(A•V$^{0.5}$). It is close to one of the slopes 2330 μN/(A•V$^{0.5}$) in this

study. Therefore, it can be concluded that the composition of ion species in the beam is an important factor to the thrust performance of the thruster, which depends on the type of propellant and the configuration of the thruster.

5.2. Asymmetry of thruster performance under positive and negative polarity

In this study, EMI-BF_4 is used as propellant. The results show that the performance of the thruster, such as emission current, mass flow rate, thrust, specific impulse and polydispersive efficiency, shows asymmetry between positive and negative modes in one test of the same thruster.

Courtney[33] observed that the collector current in positive mode is higher than that in negative mode. They attributed it to the secondary electron emission of the collector. This seems reasonable to explain the asymmetry of the collector current, but it is not feasible to explain the asymmetry of the thruster performance. Nakagawa et al.[47] also found that the current of cation is more than that of anion in their experiment. They speculated that anion beams contain more dimers (EMI-BF_4)BF_4^- or droplets than cations, but there is no TOF measurement result to prove it.

In this study, we believe that the direct reason for the asymmetry of thruster performance is the difference of ion species in the beam, and the further fundamental reason may be the different solvation energies of cations and anions. Due to the lack of more effective experimental methods, this reason may need to be further confirmed. Lozano[21] has shown that ionic liquids, as propellants of electrospray thruster, have high electrical conductivity and suitable surface tension. The electric field reaches a maximum near the tip of Taylor cone. Ion emission then occurs if this field is large enough to overcome the potential barrier given by the ion solvation energy. Many researchers have proved that ionic liquids can achieve pure ion emission.[21,48] Guerrero et al.[49] indicated that the activation energy of ionic liquids may be as low as about 1.14 eV. However, we have not found different solvation energy parameters of cations and anions. The slight variations suffice to either activate or suppress the evaporation of ions[48].

Based on the above assumptions, we speculate that due to the higher solvation energy of the anion BF_4^- of EMI-BF_4, more solvated ion clusters are formed rather than pure ions under the same electric field. This can be proved by TOF results (Fig. 10). On the other hand, the configuration of porous structure of emitter layer and reservoir layer makes the internal resistance of thruster not high enough. Courtney and Shea[36] found that when the porous material with larger pore size was used as the reservoir, heavy ion clusters were observed in negative mode, while almost pure ions in positive mode under the same configuration. When the reservoir with lower pore size was used, a near pure ion emission was achieved. This experimental phenomenon may further confirm our previous assumption.

Further, in negative mode, higher proportion of heavy ions cluster in the beam leads to lower average specific charge $\langle q/m \rangle$. According to $I \sim \langle q/m \rangle^{0.5}$, $I_{sp} \sim v \sim \langle q/m \rangle^{0.5}$ and $T \sim \langle q/m \rangle^{-0.5}$, compared with the positive mode, the current and specific impulse in negative mode are smaller and the thrust is greater. Combined with Eqs. (6)–(9), we can further come to the conclusion that the lower the average specific charge, the greater the mass flow and the lower the polydispersive efficiency. Based on the research results of Courtney and Shea,[36] if the porous material with smaller pore size is used as the reservoir, it may help to improve the asymmetry of thruster performance when the thruster is operated in an alternative polarity mode, but it may need to be at the cost of increasing the applied voltage.

6. Conclusions and outlook

In order to meet the requirements of CubeSats for micro-propulsion system, a prototype of porous ionic liquid electrospray thruster (ILET-3) is designed in this study. The performance of ILET-3 is tested in the vacuum chamber, including the following four parts: (A) general ignition test, current measurement and beam images at different voltages; (B) time of flight mass spectrometry; (C) beam angular distributions; (D) direct thrust test. The main conclusions are drawn as follows:

(1) The size of ILET-3 is 3 cm × 3 cm × 1 cm, with a total weight of about 15 g (with propellant). It can work in the voltage range of ±2.0 kV to ±3.0 kV, and the maximum emission current and input power are about 355 μA and 1.12 W in positive mode, respectively, while 250 μA and 0.91 W in negative mode, respectively. The effective divergence half angle of ILET-3 is 18.4°, which will cause about 5 % thrust loss.

(2) TOF results show that cationic monomers and dimers dominate the beam in positive mode, while there is a higher proportion of higher-order solvated ion clusters in negative mode. The maximum specific impulse and polydispersive efficiency in positive mode are 2992 s and 56.5 %, respectively, while 849 s and 43.6 % in negative mode, respectively.

(3) The thrust of ILET-3 is directly tested by torsional thrust stand. The results show that the thrust can respond quickly to the change of applied voltage in both positive and negative modes. The thrust in positive mode is 2.3–31.8 μN, and in negative mode is 2.1–42.6 μN. The thrust measured directly is in good agreement with the thrust calculated by TOF corrected by $\cos\theta_{eff}$, but the thrust trend of positive and negative modes are inconsistent.

(4) The performance of ILET-3, such as emission current, mass flow rate, thrust, specific impulse and polydispersive efficiency, shows asymmetry between positive and negative modes. We believe that the direct reason for the asymmetry of thruster performance is the difference of ion species in the beam, and the further fundamental reason may be the different solvation energies of cations and anions. Due to the lack of more effective experimental methods, this reason may need to be further confirmed.

In general, most of the performance parameters of ILET-3 are good, which can theoretically meet the requirements of CubeSats for micro-propulsion system. However, at the current stage, there are still some problems, such as asymmetric performance and large intercepted current. The asymmetric performance of the thruster may complicate the modulation mode of beam self-neutralization, and the large intercepted current will reduce the total efficiency of the thruster. Therefore, the performance of ILET-3 needs to be further improved to meet the requirements of practical application. In addition, the long-term stability of thrust and the service life of thruster also need to be further studied.

Declaration of Competing Interest

The authors declare that they have no known competing financial interests or personal relationships that could have appeared to influence the work reported in this paper.

Acknowledgements

This study was supported by the National Key R&D Program of China (No. 2020YFC2201103).

References

1. Kopacz JR, Herschitz R, Roney J. Small satellites an overview and assessment. *Acta Astronaut* 2020;**170**:93–105.
2. Yang M, Wang H, Wu CJ, et al. Space flight validation of design and engineering of the ZDPS-1A pico-satellite. *Chin J Aeronaut* 2012;**25**(5):725–38.
3. Yu ZT, Shang HB, Wei BW. Accessibility assessment and trajectory design for multiple Near-Earth-asteroids exploration using stand-alone CubeSats. *Aerosp Sci Technol* 2021;**118**:106944.
4. Poghosyan A, Golkar A. CubeSat evolution: Analyzing CubeSat capabilities for conducting science missions. *Prog Aerosp Sci* 2017;**88**:59–83.
5. Han K, Wang H, Xiang T, et al. Magnetometer compensation scheme and experimental results on ZDPS-1A pico-satellite. *Chin J Aeronaut* 2012;**25**(3):430–6.
6. Han K, Wang H, Tu BJ, et al. Pico-satellite autonomous navigation with magnetometer and Sun sensor data. *Chin J Aeronaut* 2011;**24**(1):46–54.
7. Gomez Jenkins M, Krejci D, Lozano P. CubeSat constellation management using Ionic Liquid Electrospray Propulsion. *Acta Astronaut* 2018;**151**:243–52.
8. Ling WYL, Zhang S, Fu H, et al. A brief review of alternative propellants and requirements for pulsed plasma thrusters in micro-propulsion applications. *Chin J Aeronaut* 2020;**33**(12):2999–3010.
9. Silva MAC, Guerrieri DC, Cervone A, et al. A review of MEMS micropropulsion technologies for CubeSats and PocketQubes. *Acta Astronaut* 2018;**143**:234–43.
10. Cheng YG, Xia GQ. Simulation of plasma behavior for medium propellant mass and pulsed energy of small scale pulsed inductive thruster. *Chin J Aeronaut* 2020;**33**(1):176–90.
11. Ning ZX, Liu CG, Zhu XM, et al. Diagnostic and modelling investigation on the ion acceleration and plasma throttling effects in a dual-emitter hollow cathode micro-thruster. *Chin J Aeronaut* 2021;**34**(12):85–98.
12. Macario-Rojas A, Smith KL. Spiral coning manoeuvre for in-orbit low thrust characterisation in CubeSats. *Aerosp Sci Technol* 2017;**71**:337–46.
13. Wright WP, Ferrer P. Electric micropropulsion systems. *Prog Aerosp Sci* 2015;**74**:48–61.
14. Huang CJ, Li JL, Li M. Performance measurement and evaluation of an ionic liquid electrospray thruster. *Chin J Aeronaut* 2023;36(3):1–15.
15. Chen C, Chen M, Zhou H. Characterization of an ionic liquid electrospray thruster with a porous ceramic emitter. *Plasma Sci Technol* 2020;**22**(9):94009.
16. Zhang JR, Cai GB, Liu XH, et al. Molecular dynamics simulation of ionic liquid electrospray: revealing the effects of interaction potential models. *Acta Astronaut* 2021;**179**:581–93.
17. Zhang JR, Cai GB, Shahzad A, et al. Ionic liquid electrospray behavior in a hybrid emitter electrospray thruster. *Int J Heat Mass Transf* 2021;**175**:121369.
18. Zheng WJ, Liu XH, Zhang JR, et al. Molecular dynamics simulation of ionic liquid electrospray: microscopic presentation of the effects of mixed ionic liquids. *Int J Heat Mass Transf* 2022;**182**:121983.
19. Sun W, Wu ZW, Sun ZN, et al. Study on the control of propellant flow by electric field in ionic liquid electrospray thruster. *Int J Heat Mass Transf* 2022;**183**:121926.
20. Guo Y, Li S, Wu Z. Design of ionic liquid electrospray micro-thruster system and preliminary study on its performance. *J Propuls Technol* 2020; **41**(1): 212–9 [Chinese].
21. Lozano P. Studies on the ion-droplet mixed regime in colloid thrusters [dissertation]. Cambridge: Massachusetts: Institute of Technology; 2003.
22. Lozano P, Martínez-Sánchez M. Ionic liquid ion sources: Characterization of externally wetted emitters. *J Colloid Interface Sci* 2005;**282**(2):415–21.
23. Gamero-Castaño M, Cisquella-Serra A. Electrosprays of highly conducting liquids: a study of droplet and ion emission based on retarding potential and time-of-flight spectrometry. *Phys Rev Fluids* 2021;**6**:013701.
24. Yang YT, Guo DW, Li XK, et al. Development and characterization of a novel porous-media borosilicate glass ion sources for electrospray thruster. *Aerospace* 2021;**8**(10):297.
25. Ma CY, Bull T, Ryan CN. Plume composition measurements of a high-emission-density electrospray thruster. *J Propuls Power* 2021;**37**(6):816–31.
26. Natisin MR, Zamora HL, Holley ZA, et al. Efficiency mechanisms in porous-media electrospray thrusters. *J Propuls Power* 2021;**37**(5):650–9.
27. Courtney DG, Dandavino S, Shea H. Comparing direct and indirect thrust measurements from passively fed ionic electrospray thrusters. *J Propuls Power* 2016;**32**(2):392–407.
28. Courtney DG, Shea H, Dannenmayer K, et al. Charge neutralization and direct thrust measurements from bipolar pairs of ionic electrospray thrusters. *J Spacecr Rockets* 2017;**55**(1):54–65.
29. Yang C, He JW, Duan L, et al. A torsional thrust stand for measuring the thrust response time of micro-Newton thrusters. *Int J Mod Phys A* 2021;**36**(11&12):2140015.
30. Natisin MR, Zamora HL, McGehee WA, et al. Fabrication and characterization of a fully conventionally machined, high-performance porous-media electrospray thruster. *J Micromech Microeng* 2020;**30**(11):115021.
31. Krejci D, Mier-Hicks F, Thomas R, et al. Emission characteristics of passively fed electrospray microthrusters with propellant reservoirs. *J Spacecr Rockets* 2017;**54**(2):447–58.
32. Legge R, Lozano P. Performance of heavy ionic liquids with porous metal electrospray emitters. Reston: AIAA; 2008. Report No.: AIAA-2008-5002.
33. Courtney D. Ionic liquid ion source emitter arrays fabricated on bulk porous substrates for spacecraft propulsion [dissertation]. Cambridge: Massachusetts: Institute of Technology; 2011.
34. Huang CJ, Li JL, Li M, et al. Experimental investigation on current modes of ionic liquid electrospray from a coned porous emitter. *Acta Astronaut* 2021;**183**:286–99.
35. Sun Z, Wu Z, Guo Y, et al. Plume neutralization characteristics of ionic liquid electrospray thruster. *J Propul Technol* 2021;**43**(4):200310.
36. Courtney DG, Shea H. Influences of porous reservoir Laplace pressure on emissions from passively fed ionic liquid electrospray sources. *Appl Phys Lett* 2015;**107**(10):103504.
37. Lozano PC. Energy properties of an EMI-Im ionic liquid ion source. *J Phys D: Appl Phys* 2006;**39**(1):126–34.
38. Grustan-Gutierrez E, Gamero-Castaño M. Microfabricated electrospray thruster array with high hydraulic resistance channels. *J Propuls Power* 2017;**33**(4):984–91.
39. Gamero-Castaño M, Hruby V. Electrospray as a source of nanoparticles for efficient colloid thrusters. *J Propuls Power* 2001;**17**(5):977–87.

40. Huang CJ, Li JL, Li M, et al. Emission performance of ionic liquid electrospray thruster for micropropulsion. *J Propuls Power* 2022;**38**(2):212–20.
41. Legge Jr RS, Lozano PC. Electrospray propulsion based on emitters microfabricated in porous metals. *J Propuls Power* 2011;**27**(2):485–95.
42. Liu X, Kang X, Deng H, et al. Energy properties and spatial plume profile of ionic liquid ion sources based on an array of porous metal strips. *Plasma Sci Technol* 2021;**23**(12):125502.
43. Courtney DG, Wood Z, Gray S, et al. High-speed transient characterization of the Busek BET-300-P electrospray thruster. *36th international electric propulsion conference*, 2019.
44. Natisin M, Zamora H. Performance of a fully conventionally machined liquid-ion electrospray thruster operated in PIR. *36th international electric propulsion conference*, 2019.
45. Gamero-Castaño M. Characterization of the electrosprays of 1-ethyl-3-methylimidazolium bis(trifluoromethylsulfonyl) imide in vacuum. *Phys Fluids* 2008;**20**(3):032103.
46. Chen C, Chen ML, Fan W, et al. Effects of non-uniform operation of emission sites on characteristics of a porous electrospray thruster. *Acta Astronaut* 2021;**178**:192–202.
47. Nakagawa K, Tsuchiya T, Takao Y. Microfabricated emitter array for an ionic liquid electrospray thruster. *Jpn J Appl Phys* 2017;**56**(6S1):06GN18.
48. Romero-Sanz I, Bocanegra R, Fernandez de la Mora J, et al. Source of heavy molecular ions based on Taylor cones of ionic liquids operating in the pure ion evaporation regime. *J Appl Phys* 2003;**94**(5):3599–605.
49. Guerrero I, Bocanegra R, Higuera FJ, et al. Ion evaporation from Taylor cones of propylene carbonate mixed with ionic liquids. *J Fluid Mech* 2007;**591**:437–59.